Altered cross-frequency coupling in resting-state MEG after mild traumatic brain injury

Marios Antonakakis, Stavros I. Dimitriadis, Michalis Zervakis, Sifis Micheloyannis, Roozbeh Rezaie, Abbas Babajani-Feremi, George Zouridakis, Andrew C. Papanicolaou

PII: S0167-8760(16)30019-8
DOI: doi: 10.1016/j.ijpsycho.2016.02.002
Reference: INTPSY 11081

To appear in: *International Journal of Psychophysiology*

Received date: 15 July 2015
Revised date: 23 January 2016
Accepted date: 16 February 2016

Please cite this article as: Antonakakis, Marios, Dimitriadis, Stavros I., Zervakis, Michalis, Micheloyannis, Sifis, Rezaie, Roozbeh, Babajani-Feremi, Abbas, Zouridakis, George, Papanicolaou, Andrew C., Altered cross-frequency coupling in resting-state MEG after mild traumatic brain injury, *International Journal of Psychophysiology* (2016), doi: 10.1016/j.ijpsycho.2016.02.002

Altered Cross-frequency Coupling in Resting-State MEG after Mild Traumatic Brain Injury

Marios Antonakakis[1,10], Stavros I. Dimitriadis[2,3], Michalis Zervakis[1], Sifis Micheloyannis[4], Roozbeh Rezaie[5,6], Abbas Babajani-Feremi[5,6,9], George Zouridakis[7,8,*], and Andrew C. Papanicolaou[5,6,9]

1. Digital Image and Signal Processing Laboratory, School of Electronic and Computer Engineering, Technical University of Crete, Chania, 73100, Greece
2. Artificial Intelligence and Information Analysis Laboratory, Department of Informatics, Aristotle University, Thessaloniki, 54124, Greece
3. Neuroinformatics Group, Department of Informatics, Aristotle University of Thessaloniki, Thessaloniki, Greece
4. L. Widen Laboratory, School of Medicine, University of Crete, Greece
5. Department of Pediatrics, Division of Clinical Neurosciences, University of Tennessee Health Science Center, Memphis, TN, USA
6. Neuroscience Institute, Le Bonheur Children's Hospital, Memphis, TN, USA
7. Basque Center on Cognition, Brain and Language (BCBL), Paseo Mikeletegi 69, 20009 Donostia-San Sebastián, Spain
8. Biomedical Imaging Lab, Departments of Engineering Technology, Computer Science, Biomedical Engineering, and Electrical and Computer Engineering, University of Houston, Houston, TX 77204, USA
9. Department of Anatomy and Neurobiology, University of Tennessee Health Science Center, Memphis, TN, USA
10. Corresponding author, phone: +30 28210 37206, Fax: +30 28210, 37542, email: mantonakakis@isc.tuc.gr, antonakakismar@gmail.com (Antonakakis Marios).

[*] GZ was Visiting Professor at BCBL under an Ikerbasque Fellowship during the development of this study. His permanent appointment is with the University of Houston.

Abstract

Cross-frequency coupling (CFC) is thought to represent a basic mechanism of functional integration of neural networks across distant brain regions. In this study, we analyzed CFC profiles from resting state Magnetoencephalographic (MEG) recordings obtained from 30 mild traumatic brain injury (mTBI) patients and 50 controls. We used mutual information (MI) to quantify the phase-to-amplitude coupling (PAC) of activity among the recording sensors in six nonoverlapping frequency bands. After forming the CFC-based functional connectivity graphs, we employed a tensor representation and tensor subspace analysis to identify the optimal set of features for subject classification as mTBI or control. Our results showed that controls formed a dense network of stronger local and global connections indicating higher functional integration compared to mTBI patients. Furthermore, mTBI patients could be separated from controls with more than 90% classification accuracy. These findings indicate that analysis of brain networks computed from resting-state MEG with PAC and tensorial representation of connectivity profiles may provide a valuable biomarker for the diagnosis of mTBI.

Keywords: Magnetoencephalography (MEG); mild traumatic brain injury; cross-frequency coupling, tensors, biomarkers

1. Introduction

Mild traumatic brain injury (mTBI) is the most common cause of brain insult. Typically, patients experience an initial brief change in mental state or consciousness that is followed by post-concussion symptoms (PCS) (Cassidy et al., 2004), such as headaches, fatigue, and dizziness, which usually emerge on the day of injury and persist for at least the first few days thereafter (Boccaletti et al., 2006). In most patients, cognition recovers and PCS resolve within three months. However, up to 25% of patients (Sigurdardottir et al., 2009) suffer residual PCS, long-term impairment, and sometimes disability (Levin, 2009), so that efficient identification of alterations due to mTBI becomes particularly important. Several cognitive functions are affected by mTBI, including attention (De Monte et al., 2006; Vanderploeg et al., 2005) working memory (Vanderploeg et al., 2005), episodic memory (Tsirka et al., 2011), verbal learning (De Monte et al., 2006; Ruff et al., 1989), and visual memory (Levin et al., 1987; Raskin, 2000; Ruff et al., 1989).

Conventional neuroimaging techniques, such as acute magnetic source imaging (MRI) and computed tomography (CT), have limited sensitivity in detecting physiological alterations caused by mTBI (Bigler and Orrison, 2004; Johnston et al., 2001; Kirkwood et al., 2006). Magnetoencephalography (MEG) on the other hand, is a noninvasive functional imaging technique that measures directly neuronal currents in gray matter with extraordinary (< 1 ms) temporal resolution and excellent (2–3 mm) spatial localization accuracy (Leahy et al., 1998). Consequently, during the past several years, numerous studies have attempted to develop reliable biomarkers of mTBI based on MEG (see reviews by Jeter et al., 2013, and Huang et al., 2009, 2014). Of particular interest is the analysis of resting-state MEG activity either alone (Luo et al., 2013, Zouridakis et al., 2012; Dimitriadis et al., 2015a; Li et al., 2015) or combined with diffusion tensor imaging (DTI) MRI (Huang et al., 2014).

Recent approaches to study brain function view the brain as an intricate network of complex systems with abundant interactions between local and distant areas, having the capacity to combine local specialization (segregation) with global integration (Tononi et al., 1994; Tognoli and Kelso, 2014). Fluctuations of spontaneous activity are strongly synchronized among spatially distributed neuronal

subsystems (Contreras and Steriade, 1997; Destexhe et al., 1999), suggesting that processing of stimuli is influenced by the dynamics of coherently active networks. These spatiotemporal patterns involve not only low-frequency activity within the δ (1-4 Hz) band or below (Contreras and Steriade, 1997; Destexhe et al., 1999), but also higher frequencies in the θ (4–8 Hz), α (8–12 Hz), β (13–30 Hz), and γ (>30 Hz) ranges (Steriade et al., 1996 a, b; Destexhe et al., 1999). Oscillations in these frequency bands are known to be involved in a variety of cognitive processes (Engel and Fries, 2010; Siegel et al., 2012).

One approach to understanding the dynamic nature of connections between local and distant neural assemblies is the analysis of functional and effective connectivity (Friston et al., 1994): the former captures patterns of statistical dependence, whereas the latter attempts to extract networks of causal influences of one physiological time series over another (Aertsen et al., 1989). Several studies have demonstrated changes in functional connectivity patterns after brain tumor resection (Douw et al., 2008), recovery from stroke (Gerloff et al., 2006), and traumatic brain injury (Castellanos et al., 2010; Zouridakis et al., 2012), suggesting that functional connectivity graphs (FCGs) of brain activity are sensitive to changes due to brain insult.

The MEG is a complex signal containing different interacting frequency components. Power spectrum analysis based on the Fourier, wavelet, or Gabor transform can uncover amplitude modulations within the above-defined frequencies across time. Intrinsic coupling modes (ICMs) in ongoing activity are thought to reflect the action of two different coupling mechanisms (Engel et al., 2001): one that arises from phase coupling of band-limited oscillatory signals, and another one that results from coupled aperiodic fluctuations of signal envelopes. When studying ICMs, apart from exploring the relationship between same frequency signals, it is highly interesting to also quantify functional relationships between signals of different frequencies (Jensen and Colgin, 2007; Palva and Palva, 2011; Jirsa and Muller, 2013; Dimitriadis et al., 2015c,d,2016), as this cross-frequency coupling (CFC) has been hypothesized to represent the mechanism of interaction between local and global processes and therefore it is directly related to the integration of distributed information.

Recently, different forms of cross-frequency interactions were described (Jensen and Colgin, 2007), namely power-to-power, phase-to-phase, phase-to-frequency, and phase-to-power. There is ample evidence that the last type of CFC, also called phase-amplitude modulation, occurs very often in both animals and humans in the prefrontal cortices, the hippocampus, and other distributed cortical areas (Osipova et al., 2008; Tort et al., 2008, 2009, 2010; Cohen et al., 2009a, b; Colgin et al., 2009; Axmacher et al., 2010a, b; Voytek et al., 2010).

Only a few MEG studies have considered CFC interactions at rest or during execution of active tasks. An early study (Osipova et al., 2008) reported that γ power was phase-locked to α activity over occipital brain regions at rest with eyes closed (EC). Interestingly, there was no peak in the gamma activity estimated by Fourier transform, but a clear peak was evident only when studied in relation to the alpha phase. In another MEG study (Palva et al., 2005), cross-frequency of phase synchrony was identified as the main communication mechanism between frequencies from 3 to 80 Hz. In particular, enhanced CFC phase synchrony was revealed among the α, β, and γ frequency bands during a continuous mental arithmetic task. This enhancement of CFC phase synchrony could be attributed to the integration needed among different brain areas activated during the task that were synchronized in the dominant frequency (Palva et al., 2005).

The human brain can be divided into distinct and spatially distributed functional networks (Eierud, et al., 2014). These brain networks exist at a range of spatial scales extending from microscopic neuronal networks of individual neurons and local synaptic interactions to large-scale networks of brain areas interconnected by large white matter tracts. In the present study, we focus on how large-scale intrinsic connectivity networks (ICNs) change due to mild traumatic brain injury, considering that interactions between large-scale brain networks are significant for high-level cognitive functions, such as memory and attention (Mesulam, 1998). Moreover, neuroimaging techniques, including electroencephalography (EEG), MEG, fMRI, and DTI, have recently enabled investigation of these networks in clinical populations (for a review see Eierud, et al., 2014). ICNs are composed of brain regions that are characterized by temporally coordinated activity (Beckmann et al., 2005; Smith et al., 2009). The functional architecture of these networks possibly

reflects the underlying structural brain connectivity, since brain areas strongly connected via white-matter tracts are likely to present strong functional connections. This linkage supports the assumption that ICN function is vulnerable to the effects of mTBI, considering that diffuse axonal injury (DAI) usually damages long-distance white-matter tracts that connect key brain areas (known as hubs) in these networks (Smith et al., 2003; Gentleman et al., 1995).

ICN abnormalities after TBI have been widely observed in resting-state fMRI, demonstrating both increase and decrease of connectivity in a number of networks, including the default mode network (DMN) and salience network (SN) (Sharp et al., 2011; Stevens et al., 2012). Several studies have also reported that these abnormalities correlate with cognitive impairment or post-concussive symptoms (Messe et al., 2013; Caeyenberghs et al., 2014). Recent studies based on EEG and MEG, which provide higher temporal resolution than fMRI, have further demonstrated disrupted functional connectivity related to TBI for different types of injury severity (Castellanos et al., 2010; Tarapore et al., 2013; Dimitriadis et al., 2015b).

Based on the aforementioned evidence from previous studies, we investigate the hypothesis that exploring ICMs in terms of cross-frequency coupling can provide better understanding of how mTBI alters the integration of information exchange at resting-state networks. Such alterations of oscillations, referred to as “oscillopathies” or “dysrhythmias,” could reflect malfunction and disruption of brain networks in mTBI subjects. Thus, they could assist in defining alternative or complementary connectomic biomarkers (Buzsáki and Watson, 2012).

In the present study, we demonstrate how the phase of low frequency spontaneous MEG activity modulates higher frequency activity in mTBI subjects (Florin and Bairrat, 2015). Then, adopting a phase-to-amplitude coupling (PAC) estimator to quantify CFC between pairs of frequencies, we construct cross-frequency FCGs in mTBI patients and controls. We hypothesize that PAC at rest can capture intrinsic network interactions that play a crucial role in information exchange and integration. Finally, we examine the proposition that mTBI can affect functional integration, mainly the communication between different cell assemblies

that function on a prominent frequency, and these functional changes of intrinsic networks can be captured by CFC.

The remainder of this paper is structured as follows: the next section, Methods, describes the study participants and the MEG recording procedures, the preprocessing steps for artifact detection and elimination, the dimensionality reduction algorithm, and the various classification schemes applied on the filtered FCGs. Furthermore, several methods for comparing the CFC pairs between the two groups are discussed. The following section, Results, presents the performance of each classification scheme on the current dataset and examines the differences between the two groups as potential biomarkers. The final section, Discussion, summarizes our findings, provides concluding remarks about the CFC metric and its potential use as a biomarker for mTBI, and suggests future analysis directions.

2. Methods

Our study employs network analysis of filtered directed graphs that are constructed from interacting networks that are coupled at specific frequency pairs and quantify local and global connection density in both subject groups. Cross-frequency coupling (CFC) is thought to represent a basic mechanism of functional integration of neural networks across distant brain regions. In the present study, we measure the basic type of CFC called phase-to-amplitude (PAC) coupling. After classification, which is used keep only those frequency couples with high accuracy of subject separation, we first form FCGs based on the PAC measure which are then explored for topological differences between the two groups and for their community profile.

An important step to understanding topological differences is to first estimate a basic network structure with global (functional integration) and local (functional segregation) efficiency at both network and sensor levels, and then detect consistent group-functional clusters (Rubinov and Sporns, 2010). CFC is a key mechanism of brain functionality with which two distant brain areas oscillating at their prominent frequency can communicate straightforward and quickly. To further

understand how changes of decreased local CFC correlate with possible underlying lesioned areas and if these changes represent the effects of a particular main injury site or global effects, whereby the entire brain sustained injury, we calculate patterns of intra-hemispheric CFC asymmetry and anterior-posterior anisotropy. Previous studies showed a reduction in frontal and hemispheric asymmetry in TBI patients using PET (Reuter-Lorenz et al., 2000; Levine et al., 2002). We demonstrate group differences related to the lateralization of functional strength over a hemisphere and examine the predominance of functional strength anteriorly or posteriorly.

2.1. Subjects and recording procedure

The present study is part of a larger mTBI project (Levin, 2009) supported by the Department of Defense (DoD). MTBI was defined using the guidelines of DoD (Assistant Secretary, 2007) and the American Congress of Rehabilitation Medicine (Kay et al., 1993). The project was approved by the Institutional Review Boards (IRBs) at the participating institutions and the Human Research Protection Official's review of research protocols for DoD. All procedures were compliant with the Health Insurance Portability and Accountability Act (HIPAA).

Thirty right-handed mTBI patients (29.3 ± 9.2 years of age) were recruited from three trauma centers in the greater Houston metropolitan area that participated in the larger study (Levin, 2009). The Galveston Orientation and Amnesia Test (GOAT) (Levin et al., 1979) was administered prior to obtaining informed consent to identify cognitive impairment that would preclude provision of informed consent. Inclusion criteria required the presence of a head injury occurring within the preceding 24 hours, Glasgow Coma Scale (GCS, Teasdale & Jennett, 1974) score 13-15, loss of consciousness <30 minutes including 0 minutes, post-traumatic amnesia <24 hours including 0 minutes, and a negative head CT scan. Exclusion criteria included a score on the Abbreviated Injury Scale (AIS) >3 for any body part, previous head injury requiring hospitalization, history of significant pre-existing disease, such as psychotic disorder, bipolar disorder, post-traumatic stress disorder (PTSD), past treatment for alcohol dependence or substance abuse, blood alcohol

level >80 mg/dL at the time of consent, documentation of intoxication, left-handedness, and contraindications for MRI, including claustrophobia and pregnancy. Details about subject demographics are shown in supplementary material.

The control group included fifty right-handed age- and gender-matched control subjects (29.2 ± 9.1 years of age) drawn from a normative data repository at UTHSC-Houston. Previous head injuries, history of neurologic or psychiatric disorder, substance abuse, and extensive dental work and implants incompatible with MEG were exclusion criteria for the control subjects. The research protocol received institutional approval prior to the study.

Subjects were asked to lie on a bed as still as possible with eyes closed. Approximately 5 minutes of resting-state MEG activity was recorded from each subject using a 248-channel whole-head Magnes WH3600 system (4D Neuroimaging Inc., San Diego, CA). Data were collected at a sampling rate of 1017.25 Hz and bandpass filtered in hardware between 0.1–200 Hz. Axial gradiometer recordings were transformed to planar gradiometer field approximations using the sincos method implemented in Fieldtrip (Oostenveld et al., 2011).

2.2. Data Preprocessing

The MEG data underwent artifact reduction using Matlab (The MathWorks, Inc., Natick, MA, USA) and Fieldtrip (Oostenveld et al., 2011). Filtering with a notch filter at 60 Hz was used to reduce the effects of line noise and it was followed by independent component analysis (ICA) to separate cerebral from non-cerebral activity using the extended Infomax algorithm as implemented in EEGLAB (Delorme and Makeig, 2004). The data were also whitened and reduced in dimensionality using principal component analysis with a threshold set to 95% of the total variance (Delorme and Makeig, 2004; Escudero et al., 2011; Antonakakis et al., 2013). The statistical values of kurtosis, Rényi entropy, and skewness of each independent component were used to eliminate ocular and cardiac artifacts. A component was considered an artifact if more than 20% of its values after normalization to zero mean and unit variance were outside the range [-2, +2] (Escudero et al., 2011; Dimitriadis et al., 2013a; Antonakakis et al., 2013, 2015).

2.3 Estimation of Amplitude-to-Phase Coupling

We explored cross-frequency interactions using phase-to-amplitude coupling (PAC), whereby the phase of a low-frequency rhythm modulated the amplitude of a higher-frequency oscillation (Tort et al., 2008). PAC was calculated between sensors X_i, X_j $(i, j = 1 \dots 248)$ of a multidimensional array of time series X using mutual information (MI), a nonlinear metric that measures the interdependence of the two time series X_i and X_j. The MI concept stems from information theory and offers several advantages: it is sensitive to any type of dependence between the time series including nonlinear relations and generalized synchronization; it is relatively robust to outliers, and it is measured in bits, a physically meaningful unit.

Initially, data from all sensors were filtered in several frequency bands, namely δ (0.5 – 4Hz), θ (4 – 8Hz), α (8-15Hz), β (15 – 30 Hz), γ_1 (30 – 45Hz), and γ_2 (45 – 80Hz). Then, to compute the PAC values we used the Hilbert Transform (HT) to estimate the phase ($\varphi_{f,i}$) and amplitude ($A_{f,i}$) of every filtered time series $X_{f,i}$, separately in each frequency band using

$$\varphi_{f,i} = \tan^{-1}\left(\frac{Im\left(HT\left(X_{f,i}\right)\right)}{Re\left(HT\left(X_{f,i}\right)\right)}\right) \quad (1)$$

and

$$A_{f,i} = \left|\sqrt{Im\left(HT(X_{f,i})\right)^2 + Re\left(HT(X_{f,i})\right)^2}\right| \quad (2)$$

where $\mathrm{Im}(\mathrm{HT}(X_{f,i}))$ and $\mathrm{Re}(\mathrm{HT}(X_{f,i}))$ are the imaginary and real part of $\mathrm{HT}(X_{f,i})$, respectively. We then applied a band-pass filter to $A_{f,i}$ using the same filter parameters used to extract $X_{fl,i}$, giving a new time series, $A_{fh,fl,i}$. A second Hilbert transform was then used to extract the phases of the f_l-filtered $f_{h(high)}$ amplitude envelope ($\varphi_{fh,fl,i}$) (Voytek et al., 2010).

According to the above, the mathematical definition of MI for the estimation of PAC between the phase of low frequency (f_l),$\varphi_{f_l,i}$, and the amplitude of the high frequency (f_h),$\varphi_{fh,fl,j}$, between two sensors X_i and X_j, is given by

$$PAC_{f_l,f_h}(i,j) = I\left(\varphi_{f_l,i}; \varphi_{fh,f_l,j}\right) = \sum_{y\in Y}\sum_{x\in X} p(x,y)\log\left(\frac{p(x,y)}{p_x(x)p_y(y)}\right) (3)$$

where $X = \varphi_{f_l,i}$ and $Y = \varphi_{fh,f_l,j}$, and $p(x,y)$ is the joint probability distribution function of X and Y, respectively, and $p_x(x) = \sum_{y\in Y} p(x,y)$ and $p_y(y) = \sum_{x\in X} p(x,y)$ are the marginal probability distribution functions of X and Y, respectively (Tsiaras et al., 2011).

2.4 Elements of Graph Theory

2.4.1 Topological properties of the underlying brain networks

The FCGs could be characterized based on the well-known topological metrics of *global* and *local efficiency*, established for weighted graphs and defined below, with N representing the total number of nodes in the network, E the total number of edges, and w_{ij} the weights between nodes.

Global efficiency (GE) for a network W of NxN nodes is the inverse of the harmonic mean of the shortest path length between each pair of nodes and reflects the overall efficiency of parallel information transfer in the network (Achard and Bullmore, 2007; Latora and Marchiori, 2001).

$$GE = \frac{1}{N}\sum_{i\in N}\frac{\sum_{j\in N, j\neq i}\left(d_{ij}\right)^{-1}}{N-1} (4)$$

Local efficiency (LE) is understood as a measure of fault tolerance of the network, since it indicates how well the subgraphs exchange information when a particular node is eliminated (Achard and Bullmore, 2007). Specifically, each node is assigned the shortest path length within its subgraph G_i

$$LE = \frac{1}{N}\sum_{i\in N} nodal_{LE_i} = \frac{1}{N}\sum_{i\in N}\frac{\sum_{j,h\in G_i, j,h\neq i}\left(d_{jh}\right)^{-1}}{k_i(k_i-1)} \quad (5)$$

where k_i corresponds to the total number of spatial (first level) neighbors of the i-th node, while d denotes the shortest path length.

2.4.2 **Significant links**

The aforementioned procedures result in a matrix of PAC values between the time series on all possible pairs of sensors that is modeled as a fully connected, directed, weighted, and symmetric FCG, representing causal influences among all cortical regions. The maximum number of possible directed connections N in a network with k=248 nodes is k^2=61504, and the FCG is extremely dense. Therefore, the FCG connections must be filtered out so that the pattern with the most significant connections can emerge. We performed a topological filtering based on graph theory principles and data-driven thresholding.

Topological filtering relies on graph-based analysis (Bullmore and Sporns, 2009; Bassett et al., 2009; He and Evans, 2010; Stam, 2010; Dimitriadis et al., 2010a,b,2012a,b,c,2013a,b), which is used to capture the structure of the neural system under investigation and the relationship between separation and integration of neural populations. Small-word structures are characterized by a dense network of local connections and a limited number of long-range connections that provide efficient communication between distant nodes. Efficiency in information transmission between nodes is measured as the inverse of the shortest distance between the nodes, while the average of all pair-wise efficiencies represents the global efficiency of the graph. The function cost relates to the energy expenditure needed for a network to maintain its efficiency, and it is given by the ratio of existing connections divided by the total number of possible pairwise connections in a network.

Global cost efficiency is defined as the global efficiency GE at a given cost C minus the cost (GE-C), which typically has a positive maximum value at some cost C_{max}, for an economical small-world network. Importantly, this metric of network

topology is independent of arbitrary, investigator-specified thresholds. Instead, the cost efficiency curve is estimated over a wide range of thresholds, and the behavior of the curve is summarized by its maximum value, which occurs at a data driven connection density or cost C (Bassett et al., 2009, Dimitriadis et al., 2015b). The above steps are described in the Supplementary Material and an implementation of the current approach is also available[1] (Dimitriadis et al., 2010a).

2.5 Classification of FCG Patterns

The values of the PAC matrices are considered features in a high-dimensional space that can be used to classify the FCGs obtained from individual subjects. In most studies, however, FCGs are treated as vectors in a high-dimensional space (e.g. Shen et al., 2010; Pollolini et al., 2010; Richiardi et al., 2011), an approach that disregards the inherent tabular representation of FCGs and their nature as second-order tensors. To overcome this limitation, we treat FCGs as tensors and resort to tensor subspace analysis (TSA) for appropriate feature extraction (He and Cai, 2005). In our formulation, the tensor form was given as (subjects x sensors x sensors) (Dimitriadis et al., 2013b; 2015b,c).

The TSA procedure blends multi-linear algebra and manifold data learning. Given some FCGs sampled from the space of functional connectivity patterns, the TSA approximation is modeled by first building an adjacency graph capturing the proximity relationships among the connectivity patterns and then deriving a tensor subspace that faithfully represents these relationships. TSA provides an optimal linear approximation to the FCG manifold. The entire TSA procedure is described in the supplementary material.

2.5.1 Learning machines for classification

Classification of FCGs from individual subjects starts by computing the TSA representation and is followed by comparison with FCGs of known label. In our

[1] http://users.auth.gr/~stdimitr/software.html ;

study, we used the k-NN algorithm and the Frobenius norm (Horn and Johnson, 1990) as measure of similarity. Apart from this classification scheme, indicated as "TSA+k-NN", we also employed TSA with ensemble classification ("TSA+ENS") and TSA with extreme learning machine (ELM) classification ("TSA+ELM"). The description of the "TSA+ENS" and "TSA+ELM" schemes is given in the supplementary material.

To evaluate the performance of our strategy, a cross-validation scheme was followed. The entire set of individual FCGs (control and mTBI) was randomly partitioned into two subsets, a *training set* (the database of FCGs of known class) corresponding to 80% of the subjects (45 controls and 27 mTBI patients) and a *test set* (subjects for which the class had to be predicted) corresponding to the remaining 20% of the subjects (5 controls and 3 mTBI patients). As a measure of performance we used the correct recognition rate (CC%) calculated as the proportion of subjects in the test set for which the correct label was predicted. The cross-validation scheme was repeated 100 times and the mean value and standard deviation of the overall performance, sensitivity, and specificity were estimated.

2.6 Statistical and Spatial Differences in Network Metrics

2.6.1 Statistical Analysis

Statistical analysis was performed on the GE and LE network metrics to detect significant differences between the two groups at every sensor (or total GE/LE i.e., averaged value across sensors) and frequency pair.

We adopted a sequential methodology (Antonakakis et al., 2013) for the estimation of the null hypothesis of equal means between the two groups. First, the single-sample Kolmogorov-Smirnov goodness-of-fit hypothesis test with Lilliefors correction (Conover, 1980) was employed as a test for normality to help select the appropriate type of statistical test to use (parametric t-test or non-parametric U-test). If the p-value of the normality test was under the significant level, the non-parametric Mann-Whitney U-test (Gibbons and Chakraborti, 2011) was used; otherwise, a two-sample t-test was employed. The t-test was performed with either equal or unequal variances depending on a chi-square test (F-test) for

heteroscedasticity of the samples. The threshold for significance of the p-value was set to 95%.

2.6.2 Spatially reduced representation

In order to visualize the variability and the distance between the two groups in the 3D space, a low-dimensional representation was used to visualize possible differences between control and mTBI subjects without using statistical analysis. First, GE and LE values were estimated using the Minkowski distance ($d_{st} = \sqrt[p]{\sum_{j=1}^{N}|X_{sj} - X_{tj}|^p}$ with p being a positive scalar) and the final estimates were tabulated in an 80 x 80 matrix, since the total number of subjects was 80 (50 control and 30 mTBI GE or LE values for frequency couple). Then, using multidimensional scaling (Borg & Groenen, 2005), a well-known dimensionality reduction technique, we were able to project the original multidimensional data in three dimensions. A single entry of this matrix presents an estimation of the distinction between two different nodal GE/LE profiles. The lower its value, the more alike the segregation pattern between the two subjects. We then designed a colored convex hull for each group to visualize the variability and the distance between the two groups in the 3D space. As an estimator of variability within each group, we computed the area of corresponding convex hull (Dimitriadis et al., 2015b).

2.7 Intra-hemispheric Cross Frequency Functional Coupling Asymmetry and Anterior-Posterior Anisotropy in mTBI

Possible asymmetries between the left and right hemisphere inter-dependencies based on the estimated FCGs on each frequency couple were investigated by defining the following functional-coupling asymmetry index (FAI):

$$FAI = \frac{FC_L - FC_R}{F_R} \quad (6)$$

where $\mathrm{F_L}/\mathrm{F_R}$ is the aggregate weight from all the connection-strengths among the FCG nodes restricted in either the left or right hemisphere.

Functional connectivity anisotropies between anterior and posterior brain areas based on the estimated FCGs on each frequency pair were investigated by defining the following anterior-posterior asymmetry index (API):

$$API = \frac{FC_{ant} - FC_{post}}{FC_{ant}} \quad (7)$$

where $\mathrm{FC_{ant}}/\,\mathrm{FC_{post}}$ is the aggregate weight from all the connection strengths among the FCG nodes restricted in either the left-right frontal areas or left-right parieto-occipital areas. Both subareas consisted of 58 sensors.

Figure 1 summarizes the three main steps of the proposed analysis procedure necessary to obtain FCGs and their topological parameters: first, the raw MEG recordings underwent preprocessing to eliminate non-cerebral activity; then, CFC pairs were estimated using PAC and a classification scheme performed on the filtered CFC graphs; finally, graph parameters and communities were estimated to compare the control and mTBI groups.

[Figure 1]

3 Results

3.1 Classification Performance

This section presents the results of CFC FCGs classification between the control and mTBI groups. We assessed classification performance based on the tensorial representation of FCGs with two classifiers, k-NN and ELM, and an ensemble classification scheme (ENS). Table 1 summarizes the performance of each classifier after keeping only those frequency pairs with accuracy > 90%. The control subject labels were defined as positive and the mTBI labels as negative. Both the k-

NN and ENS showed classification accuracy > 90% only in five frequency pairs, while the ELM showed similar performance only in two pairs, δ-β and β-γ_2. Also the k-NN and ENS approaches showed high sensitivity, > 90%, with specificity ranging between 85-95%. In contrast, ELM achieved lower sensitivity and specificity values. Based on these classification results, the subsequent analysis was performed only on frequency couples with accuracy > 90%.

To further validate the proposed TSA approach, we adopted LDA as a feature extraction technique applied over vectorized versions of tensorial FCGs using the same set of classifiers (see Supp. Material – Table S3). TSA demonstrated higher classification accuracy across cross-frequency pairs independently of the classifier (Table S3). Additional, nodal GE and LE estimates improved the classification accuracy in the majority of cross-frequency pairs compared to TSA analysis (Table S4).

[Table 1]

3.2 Differences in Network metrics

3.2.1 Statistical Analysis Results

Figures 2 and 3 illustrate the average global and local efficiency, GE and LE respectively, across all the subjects, separately for each sensor and group. Enlarged circles on the topographical layouts denote statistically significant differences between the two groups ($p < 0.05$) after applying the statistical analysis described in Section 2.6.1 and adjusting the p-values for multiple comparisons using the Benjamini and Yekutieli (BY) procedure (Benjamini and Yekutieli, 2001). In particular, based GE topography, the mTBI group showed an enhanced diffuse pattern over anterior-central brain areas bilaterally in δ-β (Fig.2.a) and δ-γ_1(Fig.2.b), while the control group exhibited an increased activation profile over the entire brain in β-γ_2 (Fig.2.e). Another interesting topographic difference was the abnormally activated brain area in mTBI located in right frontal regions, involving 9 sensors. This difference was detected on the basis of GE for frequency pairs θ-β (Fig.2.c), θ-γ_{11} (Fig.2.d), and β-γ_2 (Fig.2.e), and on the basis LE for all five frequency pairs (Fig.3).

Especially for the β-$\gamma_2$pair (Fig.3.e), all 9 sensors showed significantly higher segregation in the mTBI group compared to controls.

[Figure 2]

[Figure 3]

Finally, we estimated both GE and LE at the network level (averaged values across all sensors and subjects in each group) and we assessed statistically significant differences using the statistical analysis of Section 2.6.1 with a significant level of $p < 0.001$. A significant trend between the two groups was detected only for the β-γ_2 frequency pair, with controls exhibiting higher GE (Fig. 4.a) and mTBI patients higher LE values (Fig.4.b).

[Figure 4]

3.2.2 Spatial Analysis Results

Using the measures tabulated by the distance matrix and multi-dimensional scaling (MDS), we projected the 80 individual vectorial GE/LE profiles (50 control and 30 mTBI GE or LE values for frequency couples) to distinct points in a reduced 3D space to visualize the variability and distance of the two groups. To enhance our understanding of nodal LE, we focused on the δ-β and δ-γ_1 pairs (Fig. 5). The control group showed higher variability by a factor of 25 and 40 compared to mTBI for the δ-β (Fig. 5.a) and δ-γ_1 (Fig. 5.b) frequency pairs, respectively. The corresponding area (volume) of the convex hull (Fig. 5) was also higher for the control group (V=125.79 for δ-β and V=37.65 for δ-γ_1) compared to the mTBI group (V=5.11 for δ-β and V=0.89 for δ-γ_1).

[Figure 5]

3.3 CFC Asymmetry and Anterior-Posterior Anisotropy in mTBI

Figure 6 demonstrates the intra-hemispheric FAI and API indexes for each frequency pair in mTBI subjects. The most consistent results among the 30 mTBI subjects are the right lateralization of functional strength in the β-γ_2 frequency pair (Fig. 6.e; 22 out of 30 subjects) and the anterior predominance of functional strength in δ-β, δ-γ_1, θ-β, and θ-γ_1 frequency pairs in 25, 26, 25, and 24 out of 30 subjects, respectively (Figure 6.a-d).

[Figure 6]

Table 2 summarizes the distribution of asymmetries of both indexes between the left and right hemispheres and anterior-posterior brain areas in the mTBI group. Finally, functional connectivity strength (FCS) showed a significant trend for higher values in frontal brain regions bilaterally in controls in the δ-β, δ-γ_1, θ-β, and θ-γ_1 frequency pairs (Fig. 7.a-d) and higher FCS values for the mTBI patients in the β-γ_2 frequency pair (Fig. 7.e)

[Table 2]

[Figure 7]

4. Discussion

In this study, we analyzed resting-state brain networks using MEG recordings obtained from 50 controls and 30 mTBI patients, under the notion of phase-amplitude coupling. Our main goal was to investigate how cross-frequency coupling of spontaneous MEG activity is altered in mTBI patients compared to control subjects. PAC estimates show that the oscillatory activity of higher frequencies is modulated by the phase of slower spontaneous oscillations. We estimated PAC between sensors in a pair-wise fashion and between every possible pair of frequency

bands using the concept of MI. In addition, using a tensor representation for the CFC directed graphs and tensor subspace analysis for optimal feature extraction, we showed that mTBI patients could be separated from controls with more than 90% classification accuracy in the frequency couples (δ, β), (δ, γ_{11}), (θ, β), (θ, γ_1), and (β, γ_2) (Table 1). Classification performance based on relative power at the sensor level succeeded to discriminate mTBI from control subjects with only a 70% accuracy (see Supplementary Material). A prominent asymmetry between hemispheres in the interdependencies among mTBI subjects was observed with a right lateralization of FAI in the β-γ_2 frequency pair. The dominant API was observed with anterior predominance in most of frequency pairs. Additionally, estimation of FCS within bilateral frontal brain areas revealed significantly higher values for controls compared to mTBI subjects in most of frequency pairs, while significantly higher FCS values were observed in mTBI patients compared to controls in the β-γ_2 frequency pair.

The proposed classification scheme based on TSA algorithm outperformed in the majority of cross-frequency pairs the LDA dimensionality reduction algorithm (see Table S3). Complementary, manipulating the thresholded CFC FCGs on its inherent format (2^{nd} tensor - matrix) with TSA, we succeeded higher classification accuracy compared to nodal GE and LE (Table 1 vs Table S5). Our approach further validates the TSA representation of brain graphs as a valuable algorithmic tool for building reliable connectomic biomarkers in brain disorders/diseases like in mTBI. In previous studies, we employed TSA for the classification of EEG cognitive workload levels (Dimitriadis et al., 2013b,2015c) and also for analyzing intra-frequency FCGs on mTBI at resting-state MEG (Dimitriadis et al., 2015b).

A recent study (Dimitriadis et al., 2015b) analyzed the same dataset under the perspective of FCGs computed by quantifying functional connectivity between sensors using the phase-locking value (PLV) as a metric. That analysis also examined the concept of intra-frequency coupling in resting-state MEG and provided initial evidence of how it is affected by mTBI (Dimitriadis et al., 2015b). In the present study, we went a step further and explored how CFC, estimated via PAC, is affected by mTBI, in an attempt to illustrate a *communication mechanism* among frequency bands, rather than mere phase synchronization. By employing a PAC estimator for

quantifying CFC brain networks and adopting a tensorial treatment for the classification procedure, we derived biomarkers that could prove valuable for the evaluation of mTBI.

Further complex network analysis of PAC brain networks revealed significant differences between the two groups. By contrasting nodal GE and LE (Fig. 2 and Fig. 3) between the two groups, an abnormally activated brain area was revealed in mTBI subjects, located over the right frontal area, that showed high levels of integration and segregation, as quantified by GE and LE, respectively (Fig. 2.c, d, e and Fig. 3.a-e). No differences were revealed by the total GE/LE, expect for the β-γ_2 frequency pair (Fig. 4). The control group also showed a dense network of stronger local and global connections compared to mTBI in the five frequency pairs (Fig. 5).

Furthermore, we performed topological consensus clustering of the CFC values to uncover how the strength of CFC was distributed over the Euclidean distance between the sensors in the five frequency pairs across the two groups (see Supplementary Material). We found that the structure of the five most significant functional clusters in both groups differed significantly across the five frequency pairs. Specifically, for frequency pairs (δ-β), (δ-γ_1), and (θ-β), these clusters were spatially restricted in the control group compared to a more dispersed distribution in the mTBI group. Both groups demonstrated spatially scattered functional clusters in the frequency pairs (θ-γ_1) and (β-γ_2), but with different functional organization. Finally, the mean strength in controls was marginally higher compared to mTBI subjects, while mTBI showed a few strong and distant connections in the tail of the distributions (see Supplementary Material). Overall, our findings suggest a higher functional integration for controls compared to mTBI subjects.

It has already been demonstrated that CFC and (particularly) PAC play an important role in the communication between regions that produce different brain rhythms (Palva et al., 2005; Canolty et al, 2010), and constitute the principle mechanism of how local oscillatory activity of low frequency is interacting with distant brain areas functioning at higher frequency (Florin et al., 2015). Results from recent studies in both animals and humans support a mechanism that oscillations at higher frequencies are often modulated by the phase of slower phase fluctuations (Osipova et al., 2008; Tort et al., 2008, 2009, 2010; Cohen et al., 2009a, b; Colgin et

al., 2009; Axmacher et al., 2010a, b; Voytek et al., 2010). Important elements of nonlinear coupling across different frequencies reveal different types of CFC, such as phase-amplitude coupling (Tort et al., 2008, 2009, 2010; Cohen et al., 2009a,b; Colgin et al., 2009; Axmacher et al., 2010a,b), n:m phase locking (Dimitriadis et al., 2015b), and amplitude-amplitude coupling (Hipp et al., 2012; Engel et al., 2013). Cross-frequency coupling of spontaneous activity is altered during development (Pinal et al., 2015) and brain disorders/diseases due to structural and/or functional network alterations (Engel et al., 2013).

Conventional neuroimaging techniques (MRI and CT) express limited sensitivity to detecting physiological alterations caused by mTBI (Bigler and Orrison, 2004; Johnston et al., 2001; Kirkwood et al., 2006). MEG on the other hand, is a well-established technique that measures directly neuronal currents in gray matter with extraordinary temporal resolution and excellent spatial localization accuracy (Leahy et al., 1998). Numerous studies have attempted to develop reliable biomarkers of mTBI based on MEG (see reviews by Jeter et al., 2013 and Huang et al., 2009, 2014). The current study was successful in analyzing resting-state MEG activity alone (Luo et al., 2013, Zouridakis et al., 2012; Dimitriadis et al., 2015b; Li et al., 2015) revealing the side of the FCG for which the control group presented significantly different efficiency than the mTBI group (Figures 2 and 3).

Only a few MEG studies explore CFC interactions at both the resting-state and during active tasks in normal and diseased populations. Recently, Florin et al. (2015) using resting state MEG demonstrated that phase-amplitude coupling provides a mechanism for brain network formation, which reconciles previous findings and theories on long-range communication between neural populations. It confirms and extends previous findings in healthy participants of PAC as a key mechanism that support long-range brain synchronization (Palva et al., 2005; Canolty et al., 2006; Osipova, Hermes, and Jensen, 2008).

Topologically, our study revealed significant trends regarding the functional strength of CFC interactions. An anterior predominance of FCS (API) in δ-β, δ-γ_1, θ-β, and θ-γ_1 frequency pairs was observed (Figure 6.a-d) in the majority of mTBI subjects (25, 26, 25, and 24 out of 30 subjects, respectively). Moreover, consistent results among the 30 mTBI subjects were obtained for the right lateralization of functional

strength in the β-γ_2 frequency couple (Figure 6.e; 22 out of 30 subjects). Finally, FCS within bilateral frontal brain regions showed significant higher values for control over mTBI subjects in δ-β, δ-γ_1, θ-β, and θ-γ_1 (Fig.7.a-d) and a higher FCS for mTBI over control subjects in β-γ_2 (Fig.7.e). Our findings demonstrate that frontal brain areas are more vulnerable to brain injury and this is reflected by the lower FCS observed in mTBI subjects compared to controls in four frequency pairs (Fig. 7) (Eierud et al., 2014). These findings based on the δ band being the modulating frequency could reflect a lower deactivation of default mode network for mTBI subjects and could be attributed to inhibitory mechanisms activated at resting-state (Dimitriadis et al., 2010b). Findings based on the θ band being the modulating frequency could be related with a lower activated level of working memory at rest for mTBI, which can be interpreted as a lower reflex stand-by level ready to be activated during a cognitive task (D'Esposito et al., 1995). The role of activity in the β frequency is less studied and understood. A recent review suggested that activity in the β frequency band might be associated with the maintenance of motor sets and cognition (Engel and Fries, 2010). The significantly higher FCS for mTBI compared to controls in β-γ_2 may be associated with a balanced mechanism of the brain to keep the cognition on a quasi-normal level.

In summary, this study first demonstrated that the orchestration of resting-state brain networks is inefficient in mTBI subjects and the key mechanism of this collapse is CFC. Moreover, treating cross-frequency FCGs as tensors, along with internal cross-validation on five frequency pairs, succeeded in separating mTBI subjects from controls with higher than 90% classification accuracy. At a later stage, and using the trained classifier from this dataset, we will test its efficiency on predicting the labels of unknown external datasets. Therefore, MEG-CFC brain networks computed with PAC at rest with a tensorial representation could form a valuable connectomic biomarker for the diagnosis of mTBI.

To provide a robust mapping between brain function at the resting state and during cognition in both healthy and disease subjects, it is necessary to adopt a dynamic functional connectivity approach (Dimitriadis et al., 2010a, 2012a,b,c, 2013a, 2015a) through the definition of functional connectivity microstates (Dimitriadis et al., 2013a,c,2015a,d) and/or network microstates (Dimitriadis et al.,

2013a,c,2015a). Our future studies with mTBI subjects will focus on dynamic cross-frequency coupling, their related microstates, and their symbolic dynamical signature on MEG resting state.

Acknowledgment

The project reported here is part of a larger study, the Integrated Clinical Protocol, conducted by the Investigators and staff of The Mission Connect Mild Traumatic Brain Injury Translational Research Consortium and supported by the Department of Defense Congressionally Directed Medical Research Program. The graph representation and analysis is supported by a THALES project (CYBERSENSORS – High Frequency Monitoring System for Integrated Water Resources Management of Rivers) funded by the NSRF2007-13 of the Greek Ministry of Development. The analysis methodology was partly supported by the "YPERTHEN" project under the Interreg framework of Greek-Cyprus Co-operation 2007-2013.

References

Achard, S., Bullmore, E., 2007. Efficiency and cost of economical brain functional networks. PLoS Comput Biol 3, e17.

Aertsen, A., Gerstein, G.L., Habib, M.K., Palm, G., 1989. Dynamics of neuronal firing correlation: modulation of effective connectivity. J of Neurophysiology 61, 900–917.

Antonakakis, M., Giannakakis, G., Tsiknakis, M., Micheloyannis, S. and Zervakis, M., 2013. Synchronization coupling investigation using ICA cluster analysis in resting MEG signals in Reading Difficulties. Bioinfo and Bioeng (BIBE), 2013 IEEE 13th International Conference on, 1-5.

Antonakakis, M., Dimitriadis, S.I., Zervakis, M., Rezaie, R., Babajani-Feremi, A., Micheloyannis, S., Zouridakis, G., Papanicolaou, A.C, 2015. Comparison of brain network models using cross-frequency coupling and attack strategies. Conf Proc IEEE Eng Med Biol Soc. 7426-9.

Axmacher, N., Cohen, M.X., Fell, J., Haupt, S., Dümpelmann, M., Elger, C.E., 2010a. Intracranial EEG correlates of expectancy and memory formation in the human hippocampus and nucleusaccum- bens. Neuron 65, 541–549.

Axmacher, N., Henseler, M.M., Jensen, O., Weinreich, I., Elger, C.E., and Fell, J., 2010b. Cross-frequency coupling supports multiitem working memory in the human hippocampus. *Proc.Natl.Acad. Sci.U.S.A.* 107, 3228–3233.

Bassett, D.S., Bullmore, E.T., Meyer-Lindenberg, A., Apud, J.A., Weinberger, D.R., Coppola, R., 2009. Cognitive fitness of cost-efficient brain functional networks. Proc. Natl. Acad. Sci. USA 106, 11747–11752.

Beckmann, C. F., DeLuca, M., Devlin, J. T., Smith, S. M., 2005. Investigations into resting-state connectivity using independent component analysis. Philos. Trans. R. Soc. Lond. B Biol. Sci. 360, 1001–101.

Bigler, E.D., Orrison, W.W., 2004. Neuroimaging in sports-related brain injury. In: Lovell, M. R., Echemendia, R.J., Barth, J.T., Collins, M.W. (Eds.), Traumatic Brain Injury in Sports: An International Perspective. Lisse, Netherlands, Swets and Zeitlinger, 71–94.

Boccaletti, S., Latora, V., Moreno, Y., Chavez, M., Hwang, D.U., 2006. Complex networks: Structure and dynamics. Phys Rep 424, 175-308.

Bullmore, E., Sporns O., 2009. Complex brain networks: graph theoretical analysis of structural and functional systems. Nature Reviews Neuroscience 10, 186-198.

Caeyenberghs, K., Leemans, A., Leunissen, I., Gooijers, J., Michiels, K., Sunaert, S., Swinnen, S.P., 2014. Altered structural networks and executive deficits in traumatic brain injury patients. Brain Struct. Funct. 219, 193–209 (2014).

Canolty, R.T. and Knight, R.T, 2010. The functional role of cross-frequency coupling, Trends Cogn. Sci. 14(11), 506-15.

Cassidy, J.D., Carroll, L.J., Peloso, P.M., Borg, J., von Holst, H., Holm, L., 2004. WHO Collaborating Centre Task Force on Mild Traumatic Brain, Injury, Incidence, risk factors and prevention of mild traumatic brain injury: results of the WHO Collaborating Centre Task Force on Mild Traumatic Brain Injury. J Rehabil Med 36(43), 28-60.

Castellanos, N.P., Paul, N., Ordoñez, V.E., Demuynck, O., Bajo, R., Campo, P., Bilbao, A., Ortiz, del Pozo, F., Maestú, F., 2010. Reorganization of functional connectivity as a correlate of cognitive recovery in acquired brain injury. Brain 133, 2365–2381.

Cohen, M.X., Axmacher, N., Lenartz, D., Elger, C.E., Sturm, V. and Schlaepfer, T.E., 2009a. Good vibrations: cross-frequency coupling in the human nucleus accumbens during reward processing. *J. Cogn. Neurosci.* 21, 875–889.

Cohen, M.X., Elger, C.E., and Fell, J., 2009b. Oscillatory activity and phase-amplitude coupling in the human medial frontal cortex during decision making. *J. Cogn. Neurosci.* 21, 390–402.

Colgin, L.L., Denninger, T., Fyhn, M., Hafting, T., Bonnevie, T., Jensen, O., 2009. Frequency of gamma oscillations routes flow of information in the hippocampus. *Nature* 462, 353–357.

Conover, W.J., 1980. Practical Nonparametric Statistics. Hoboken, NJ: John Wiley & Sons, Inc.

Contreras, D., and Steriade, M., 1997. Synchronization of low-frequency rhythms in corticothalamic networks. Neuroscience 76, 11–24.

D'Esposito, M., Detre, J.A., Alsop, D.C., Shin, R.K., Atlas, S., 1995. The neural basis of the central executive system of working memory. Nature 378, 279–281.

De Monte, V.E., Geffen, G.M., Massavelli, B.M., 2006. The effects of post-traumatic amnesia on information processing following mild traumatic brain injury. Brain Inj. 20, 1345–1354.

Delorme, A., Makeig, S., 2004. EEGLAB: an open source toolbox for analysis of single-trial EEG dynamics including independent component analysis. J. Neurosci. Methods 134, 9-21.

Destexhe, A., Contreras, D., and Steriade, M., 1999. Spatiotemporal analysis of local field potentials and unit discharges in cat cerebral cortex during natural wake and sleep states. J. Neurosci. 19, 4595–4608.

Dietterich, T.G. Ensemble methods in machine learning. In: Proceedings of Multiple Classifier.

Dimitriadis, S.I., Laskaris, N.A., Del Rio-Portilla, Y., Koudounis, G.C., 2009. Characterizing dynamic functional connectivity across sleep stages from EEG. Brain Topography, 22, 119-133.

Dimitriadis, S.I., Laskaris, N.A., Tsirka, V., Vourkas, M., Micheloyannis, S., Fotopoulos, S., 2010a. Tracking brain dynamics via time-dependent network analysis. Journal of Neuroscience Methods 193(1), 145-155.

Dimitriadis, S.I., Laskaris, N.A., Tsirka, V., Vourkas, M., Micheloyannis, S., 2010b. What does delta band tell us about cognitive Processes: a mental calculation study? Neuroscience Letters 483 (1), 11-15.

Dimitriadis, S.I., Laskaris, N.A., Tsirka, V., Vourkas, M., Micheloyannis, S. 2012a. An EEG study of brain connectivity dynamics at the resting state. Nonlinear Dynamics, Psychology and Life Sciences 16(1), 5-22.

Dimitriadis, S.I., Kanatsouli, K., Laskaris, N.A., Tsirka, V., Vourkas, M., Micheloyannis, S., 2012b. Surface EEG shows that Functional Segregation via Phase Coupling contributes to the neural Substrate of Mental Calculations. Brain and Cognition, 80(1), 45–52.

Dimitriadis, S.I., Laskaris, N.A., Tzelepi, A., Economou, G., 2012c. Analyzing Functional Brain Connectivity by means of Commute Times: a new approach and its application to track event-related dynamics. IEEE (TBE) Transactions on Biomedical Engineering, 59(5), 1302-1309.

Dimitriadis, S.I., Laskaris, N.A., Tzelepi A., 2013a. On the quantization of time-varying phase synchrony patterns into distinct Functional Connectivity Microstates (FCμstates) in a multi-trial visual ERP paradigm, (3), 397-409

Dimitriadis, S.I., Sun, Yu, Kwok K., Laskaris, N.A., Thakor, N., Bezerianos, A., 2013b. A tensorial approach to access cognitive workload related to mental arithmetic from EEG functional connectivity estimates. Conf Proc IEEE Eng Med Biol Soc. 2013:2940-3.

Dimitriadis, S.I., Laskaris, N.A., P.G. Simos, S. Micheloyannis, J.M. Fletcher, R. Rezaie, Papanicolaou, A.C.,2013c. Altered temporal correlations in resting-state connectivity fluctuations in children with reading difficulties detected via MEG. NeuroImage 83: 307–31.

Dimitriadis, S.I., Laskaris, N.A., Micheloyannis S., 2015a. Dynamics of EEG-based Network Microstates unmask developmental and task differences during mental arithmetic and resting wakefulness. Cogn Neurodyn 9(4):371-387.

Dimitriadis, S.I., Zouridakis, G., Rezaie, R., Babajani-Feremi, A., Papanicolaou, A.C., 2015b. Functional connectivity changes detected with magnetoencephalography after mild traumatic brain injury, NeuroImage: Clinical, 9:519-531.

Dimitriadis, S.I., Sun, Yu, Kwok K., Laskaris, N.A., Thakor, N., Bezerianos, A., 2015c. Cognitive Workload Assessment Based on the Tensorial Treatment of EEG Estimates of Cross-Frequency Phase Interactions. Ann Biomed Eng. 43(4):977-89.

Dimitriadis, S.I., Laskaris, N.A., Bitzidou, M.P., Tarnanas, I. and Tsolaki, M.N., 2015d. A novel biomarker of amnestic MCI based on dynamic cross-frequency coupling patterns during cognitive brain responses. Front. Neurosci. 9:350. doi: 10.3389/fnins.2015.00350

Dimitriadis, S.I., Sun, Yu, Kwok K., Laskaris, N.A., Thakor, N., Bezerianos, A., 2016. Revealing cross-frequency causal interactions via a vector-quantization symbolic transfer entropy: an application to EEG recordings during a mental arithmetic task," IEEE Transactions on Neural System and Rehabilitation Engineering. In Press DOI 10.1109/TNSRE.2016.2516107

Douw, L., Baayen, H., Bosma, I., Klein, M., Vandertop, P., Heimans, J., et al., 2008. Treatment-related changes in functional connectivity in brain tumor patients: a magnetoencephalography study. Exp. Neurol. 212, 285–290.

Eierud, C, Craddock, R.C., Fletcher, S, 2014. Neuroimaging after mildtraumatic brain injury: review andmeta-analysis. Neuroimage Clin. 4, 283–94.

Eierud, C., Craddock R. C., Fletchere, S., Aulakhe, M., King-Casasa, B., Kuehlg, D., LaConte S. M., 2014. Neuroimaging after mild traumatic brain injury: Review and meta-analysis. NeuroImage: Clinical 4:283–294.

Engel, A.K., and Fries, P., 2010. Beta-band oscillations—signalling the status quo? Curr. Opin. Neurobiol. 20, 156–165.

Engel, A.K., Fries, P., and Singer, W., 2001. Dynamic predictions: oscillations and synchrony in top-down processing. Nat. Rev. Neurosci. 2, 704–716.

Engel, A.K., Gerloff, C., Hilgetag, C.C., Nolte, G., 2013. Intrinsic coupling modes: multiscale interactions in ongoing brain activity. Neuron 80, 867–886.

Escudero, J., Hornero, R., Abásolo, D., Fernández, A., 2011: Quantitative evaluation of artifact removal in real magnetoencephalogram signals with blind source separation. Ann Biomed Eng 39(8), 2274-86.

Florin, E, Baillet, S, 2015. The brain's resting-state activity is shaped by synchronized cross-frequency coupling of neural oscillations. Neuroimage, 111, 26-35.

Friston, K.J., Tononi, G., Reeke Jr., G.N., Sporns, O., Edelman, G.M., 1994. Value dependent selection in the brain: simulation in a synthetic neural model. Neuroscience 59 (2), 229–243.

Gentleman, S. M., Roberts, G. W., Gennarelli, T.A., Maxwell, W. L., Adams, J. H., Kerr, S., Graham D. I., 1995. Axonal injury: a universal consequence of fatal closed head injury? Acta Neuropath. 89, 537–543.

Gerloff, C., Bushara, K., Sailer, A., Wassermann, E.M., Chen, R., Matsuoka, T., Waldvogel, D., Wittenberg, G.F., Ishii, K., Cohen, L.G., Hallett, M., 2006. Multimodal imaging of brain reorganization in motor areas of the contralesional hemisphere of well recovered patients after capsular stroke. Brain 129 (Pt 3), 791–808.

Gibbons, J.D. and Chakraborti, S., 2011: Nonparametric Statistical Inference, 5th Ed., Boca Raton, FL: Chapman & Hall/CRC Press, Taylor & Francis Group.

Han, K., Mac Donald C. L., Johnson A. M., Barnes Y., Wierzechowski L., Zonies D., Oh J., Flaherty S., Fang R., Raichle M. E., Brody D. L., 2014. Disrupted modular organization of resting-state cortical functional connectivity in U.S. military personnel following concussive 'mild' blast-related traumatic brain injury. NeuroImage 84, 76-96.

He, Y. and Evans, A., 2010. Graph theoretical modeling of brain connectivity. Current opinion in neurology 23(4), 341-350.

Hipp, J.F., Hawellek, D.J., Corbetta, M., Siegel, M., and Engel, A.K., 2012. Large-scale cortical correlation structure of spontaneous oscillatory activity. Nat. Neurosci. 15, 884–890.

Huang, et al., 2014. Single-subject-based whole-brain MEG slow-wave imaging approach for detecting abnormality in patients with mild traumatic brain injury. NeuroImage: Clinical 5, 109–119.

Huang, M.X., Theilmann, R.J., Robb, A., Angeles, A.,Nichols, S.,Drake, A., D'Andrea, J., Levy,M., Holland, M., Song, T., Ge, S., Hwang, E., Yoo, K., Cui, L., Baker, D.G., Trauner, D., Coimbra, R., Lee, R.R., 2009. Integrated imaging approach with MEG and DTI to detect mild traumatic brain injury in military and civilian patients. J. Neurotrauma 26, 1213–1226.

Jensen, O., and Colgin, L.L., 2007. Cross-frequency coupling between neuronal oscillations. Trends Cogn. Sci. 11, 267–269.

Jeter, C.B., Hergenroeder, G.W., Hylin, M.J., Redell, J.B., Moore, A.N., Dash, P.K., 2013. Biomarkers for the diagnosis and prognosis of mild traumatic brain injury/concussion. J. Neurotrauma 30, 657–670.

Jirsa, V, Müller V, 2013. Cross-frequency coupling in real and virtual brain networks. Front Comput Neurosci., 7:78.

Johnston, K.M., Ptito, A., Chankowsky, J., Chen, J.K., 2001. New frontiers in diagnostic imaging in concussive head injury. Clin. J. Sport Med. 11, 166–175.

Kay, T., Harrington, D.E., Adams, R., Anderson, T., Berrol, S., Cicerone, K., Dahlberg, C., Gerber, D., Goka, R., Harley, P., Hilt, J., Horn, L., Lehmkuhl, D., Malec, J., 1993. Definition of mild traumatic brain injury. J. Head Trauma Rehabil. 8, 86–87.

Kirkwood, M.W., Yeates, K.O., Wilson, P.E., 2006. Pediatric sport-related concussion: a review of the clinical management of an oft-neglected population. Pediatrics 117, 1359–1371.

Leahy, R.M., Mosher, J.C., Spencer, M.E., Huang, M.X., Lewine, J.D., 1998. A study of dipole localization accuracy for MEG and EEG using a human skull phantom. Electroencephalogr. Clin. Neurophysiol. 107, 159–173.

Levin, H.S., 2009. Mission Connect Mild TBI Translational Research Consortium. Baylor College of Medicine Houston TX.

Levin, H.S., Mattis, S., Ruff, R.M., Eisenberg, H.M., Marshall, L.F., Tabaddor, K., High, Jr. W.M., Frankowski R.F., 1987. Neurobehavioral outcome following minor head injury: a three-center study. J. Neurosurg. 66, 234–243.

Levin, H.S., O'Donnell, V.M., Grossman, R.G., 1979. The Galveston Orientation and Amnesia Test. A practical scale to assess cognition after head injury. J Nerv Ment Dis. 167(11), 675-84.

Levine, B., Cabeza, R., McIntosh, A.R., Black, S.E., Grady, C.L., Stuss, D.T., 2002. Functional reorganisation of memory after traumatic brain injury: a study with H2150 positron emission tomography. J Neurol Neurosurg Psychiatry 73, 173-181.

Li, L., Pagnotta, M.F., Arakaki, X., Tran, T., Strickland, D., Harrington M., and, Zouridakis G., 2015. Brain Activation Profiles in mTBI: Evidence from Combined Resting-State EEG and MEG Activity, Conf Proc IEEE Eng Med Biol Soc., August 25-29, 2015, accepted.

Luo, Q., Xu, D., Roskos, T., Stout, J., Kull, L., Cheng, X., Whitson, D., Boomgarden, E., Gfeller, J., Bucholz, R.D., 2013. Complexity analysis of resting state magnetoencephalography activity in traumatic brain injury patients. J. Neurotrauma 30, 1702–1709.

Messé, A., Caplain, S., Pélégrini-Issac, M., Blancho, S., Lévy, R., Aghakhani, N., Montreuil, M., Benali, H., Lehéricy, S., 2013. Specific and evolving resting-state network alterations in post-concussion syndrome following mild traumatic brain injury. PLoS ONE 8, e65470.

Mesulam, M. M, 1998. From sensation to cognition. Brain 121, 1013–1052.

Oostenveld, R., Fries, P., Maris E., Schoelen, J.M., 2011. Fieldtrip: Open source software for advanced analysis ofmeg, eeg, and invasive electrophysiological data. Computational Intelligence and Neuroscience 2011 (Article ID 156869), 9 pages.

Osipova, D., Hermes, D., and Jensen, O., 2008. Gamma power is phase-locked to posterior alpha activity. *PLoSONE* 3, 7.

Palva, J.M. et al., 2005. Phase synchrony among neuronal oscillations in the human cortex. J. Neurosci. 25, 3962–3972.

Palva, J.M., and Palva, S., 2011. Roles of multiscale brain activity fluctuations in shaping the variability and dynamics of psychophysical performance. Prog. Brain Res. 193, 335–350.

Pinal, D., Zurróna, M., Díaza, F, Sauseng, P., 2015. Stuck in default mode: inefficient cross-frequency synchronization may lead to age-related short-term memory decline. Neurobiology of aging.

Raskin, S.A., 2000. Memory. In: Raskin, S.A., Mateer, C.A. (Eds.), Neuropsychological Management of Mild Traumatic Brain Injury. Oxford University Press, New York, 93–107.

Reuter-Lorenz, P.A., Jonides, J., Smith, E.E., et al., 2000. Age differences in the frontal lateralization of verbal and spatial working memory revealed by PET. J. Cogn. Neurosci. 12, 174–87.

Richiardi, J., Eryilmaz, H., Schwartz, S., Vuilleumier, P., Van De Ville D., 2011. Decoding brain states from fMRI connectivity graphs. Neuroimage 56(2), 616-626.

Rubinov M, Sporns, O, 2010. Complex network measures of brain connectivity: Uses and interpretations. NeuroImage, 52, 1059-69.

Ruff, R.M., Levin, H.S., Mattis, S., High Jr., W.M., Marshall, L.F., Eisenberg, H.M., Tabaddor, K., 1989. Recovery of memory after mild head injury: a three-center study. In: Levin, H.S., Eisenberg, H.M., Benton, A.L. (Eds.), Mild Head Injury. Oxford University Press, New York, 176–188.

Sharp, D. J., Beckmann, C. F., Greenwood, R., Kinnunen, K. M., Bonnelle, V., De Boissezon, X., Powell, J. H., Counsell, C. J., Patel, M. C., Leech, R., 2011. Default mode network functional and structural connectivity after traumatic brain injury. Brain 134, 2233–2247.

Sharp, D. J., Scott G., Leech, R., 2014. Network dysfunction after traumatic brain injury. Nature Reviews Neurology 10, 156–166.

Shen, H., Wang, L., Liu, Y., Hu, D., 2010. Discriminative analysis of resting-state functional connectivity patterns of schizophrenia using low dimensional embedding of fMRI. Neuroimage 49(4), 3110-3121.

Siegel, M., Donner, T.H., and Engel, A.K., 2012. Spectral fingerprints of largescale neuronal interactions. Nat. Rev. Neurosci. 13, 121–134.

Sigurdardottir, S., Andelic, N., Roe, C., Jerstad, T., Schanke, A.K., 2009. Post-concussion symptoms after traumatic brain injury at 3 and 12 months post-injury: a prospective study. Brain Injury 23(6), 489-497.

Smith, D. H., Meaney, D. F. & Shull, W. H., 2003. Diffuse axonal injury in head trauma. J. Head Trauma Rehabil. 18, 307–316.

Smith, S. M. et al., 2009. Correspondence of the brain's functional architecture during activation and rest. Proc. Natl Acad. Sci. USA 106, 13040–13045.

Stam, C.J., 2010. Characterization of anatomical and functional connectivity in the brain: a complex networks perspective. International Journal of Psychophysiology 77(3), 186-194.

Steriade, M., Amzica, F., and Contreras, D. 1996a. Synchronization of fast (30-40 Hz) spontaneous cortical rhythms during brain activation. J. Neurosci. 16, 392–417.

Steriade, M., Contreras, D., Amzica, F., and Timofeev, I. (1996b). Synchronization of fast (30-40 Hz) spontaneous oscillations in intrathalamic and thalamocortical networks. J. Neurosci. 16, 2788–2808.

Stevens, M. C., Lovejoy, D., Jinsuh, K., Howard O., Inam, K., SuzanneT, W., 2012. Multiple resting state network functional connectivity abnormalities in mild traumatic brain injury. Brain Imaging Behav. 6, 293–318.

Teasdale, G., Jennett, B., 1974. Assessment of coma and impaired consciousness. A practical scale. Lancet. 2(7872), 81-4.

Tognoli, G., and Scott Kelso, J.A., 2014.Enlarging the scope: grasping brain complexity. Frontiers of Systems Neuroscience.

Tononi, G., Sporns, O., and Edelman, G.M., 1994. A measure for brain complexity: relating functional segregation and integration in the nervous system. *Proc. Natl. Acad. Sci. USA* 91, 5033–5037.

Tort, A.B.L., Komorowski, R., Eichenbaum, H., and Kopell, N., 2010. Measuring phase-amplitude coupling between neuronal oscillations of different frequencies. *J. Neurophysiol.* 104, 1195–1210.

Tort, A.B.L., Komorowski, R.W., Manns, J.R., Kopell, N.J., and Eichenbaum, H., 2009. Theta–gamma coupling increases during the learning of item–context associations. *Proc. Natl. Acad. Sci. U.S.A.* 106, 20942–20947.

Tort, A.B.L., Kramer, M.A., Thorn, C., Gibson, D. J., Kubota, Y., Graybiel, A. M., 2008. Dynamic cross-frequency couplings of local field potential oscillations in ratstriatum and hippocampus during performance of aT-mazetask. *Proc.Natl.Acad.Sci.U.S.A.* 105, 20517–20522.

Tsiaras, V., Simos, P.G., Rezaie, R., Sheth, B.R., Garyfallidis, E., Castillo, E.M., et al., 2011. Extracting biomarkers of autism from MEG resting-state functional connectivity networks. Comput. Biol. Med. 41, 1166–1177.

Tsirka, V, Simos, P.G, Vakis, A., Kanatsouli, K., Vourkas, M., Erimaki, S., Pachou, E., Stam, C.J., Micheloyannis, S., 2011. Mild traumatic brain injury: Graph-model characterization of brain networks for episodic memory. Int. J. of Psychophysiol. 79, 89–96.

Vanderploeg, R.D., Curtiss, G., Belanger, H.G., 2005. Long-term neuropsychological outcomes following mild traumatic brain injury. J. Int. Neuropsychol. Soc. 11, 228–236.

Voytek, B., Canolty, R.T., Shestyuk, A., Crone, N. E., Parvizi, J., Knight, R. T., 2010. Shifts in Gamma Phase–Amplitude Coupling Frequency from Theta to Alpha Over Posterior Cortex During Visual Tasks. Front. Hum. Neurosci. 4, 191.

Zouridakis, G., Paditar, U., Situ, N., Rezaie, R., Castillo, E., Levin, H., Papanicolaou, A.C., 2012. Functional Connectivity Changes in Mild Traumatic Brain Injury Assessed Using Magnetoencephalography. J of Mechanics in Medicine and Biology 12(02).

Figure 1. The main steps of the proposed analysis procedure to estimate FCGs and their topological parameters.

Figure 2. Group-averaged global efficiency (GE) across subjects for every sensor in control and mTBI subjects for each pair of frequency bands. Larger circles with a black marker represent statistically significant differences between the two groups ($p < 0.05$).

Figure 3. Group-averaged local efficiency (LE) across subjects for every sensor in control and mTBI subjects for each pair of frequency bands. Larger circles with a black marker denote statistically significant differences between the two groups ($p < 0.05$).

Figure 4. Global (GE) and local efficiency (LE) in control and mTBI subjects across the studied frequency pairs (*$p < 0.01$).

Figure 5. The illustration of convex hull of the multidimensional scaling reduction to visualize better the total separation of segregated patterns from all subjects for δ-β and δ-γ_1, respectively. Label V denotes the area (volume) of the convex hull.

Figure 6. The intra-hemispheric Functional-Coupling Asymmetry (FAI) and anterior-posterior anisotropy (API) in mTBI subjects for each frequency couple.

Figure 7. Significant differences of bilateral frontal functional connectivity strength between controls and mTBI patients ($p < 0.01$, Wilcoxon rank-sum test; $p' < p/5$; Bonferroni corrected).

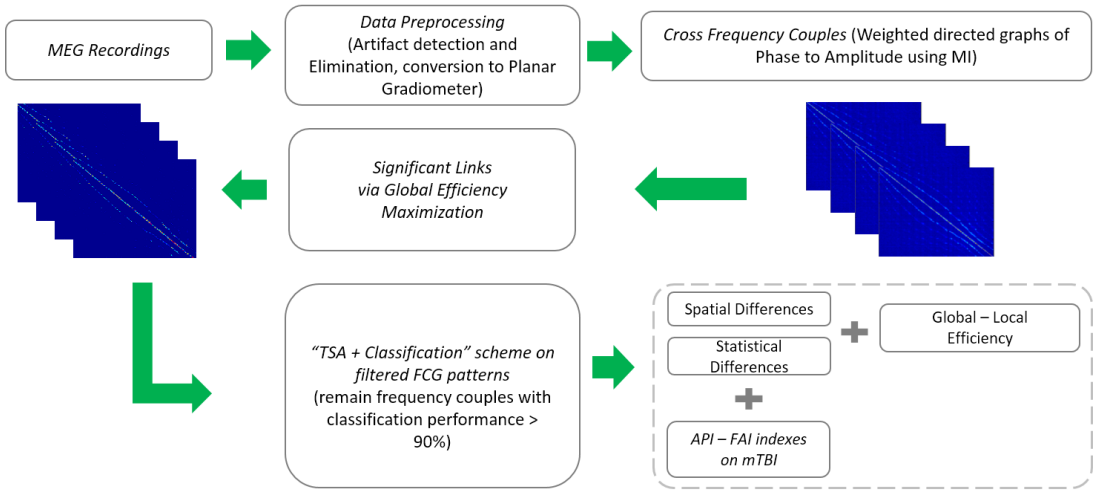

Fig. 1

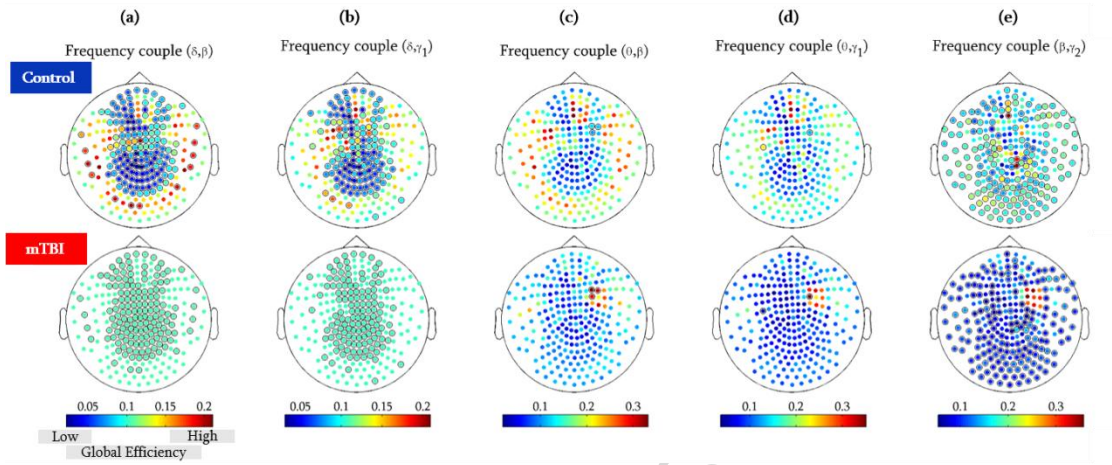

Fig. 2

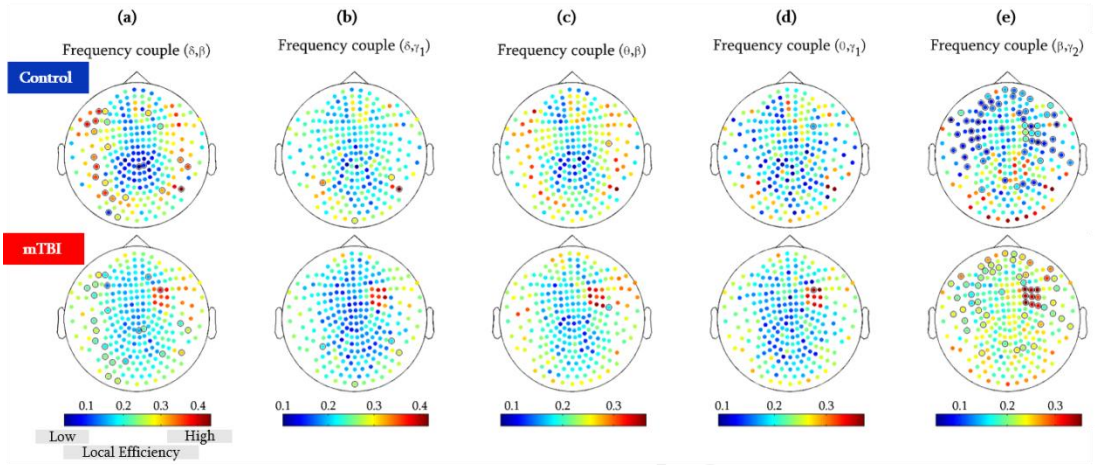

Fig. 3

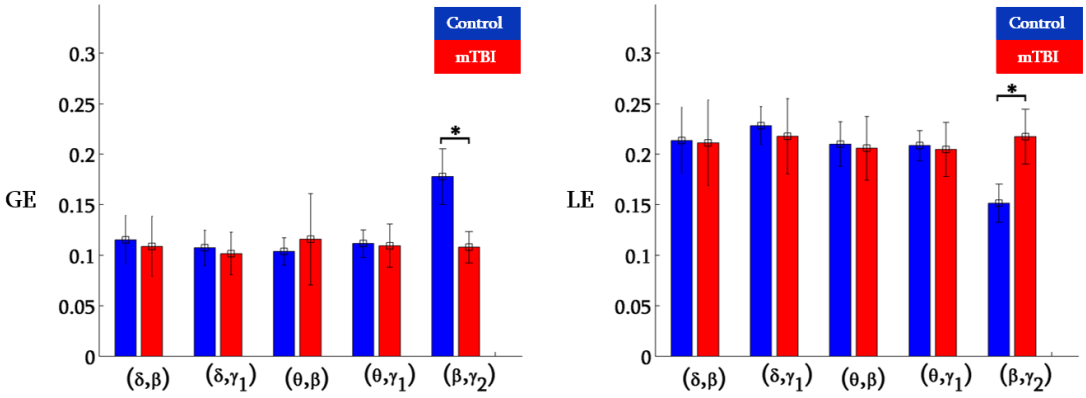

Fig. 4

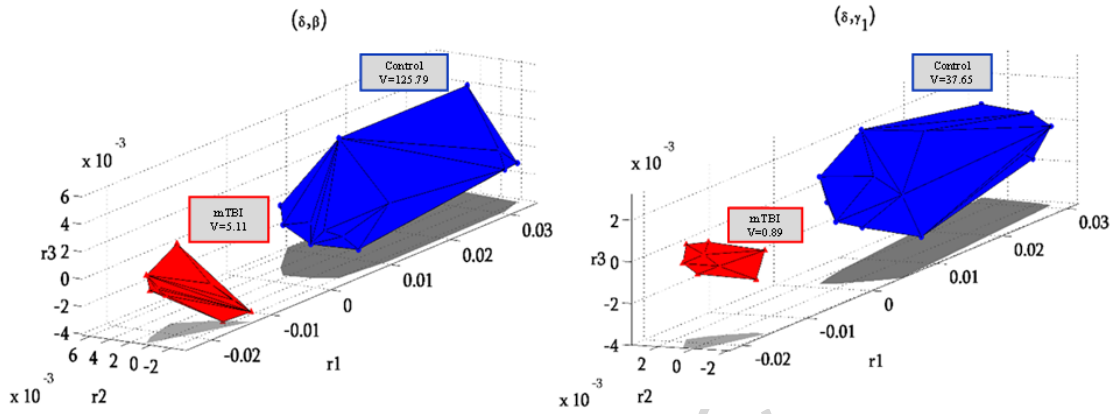

Fig. 5

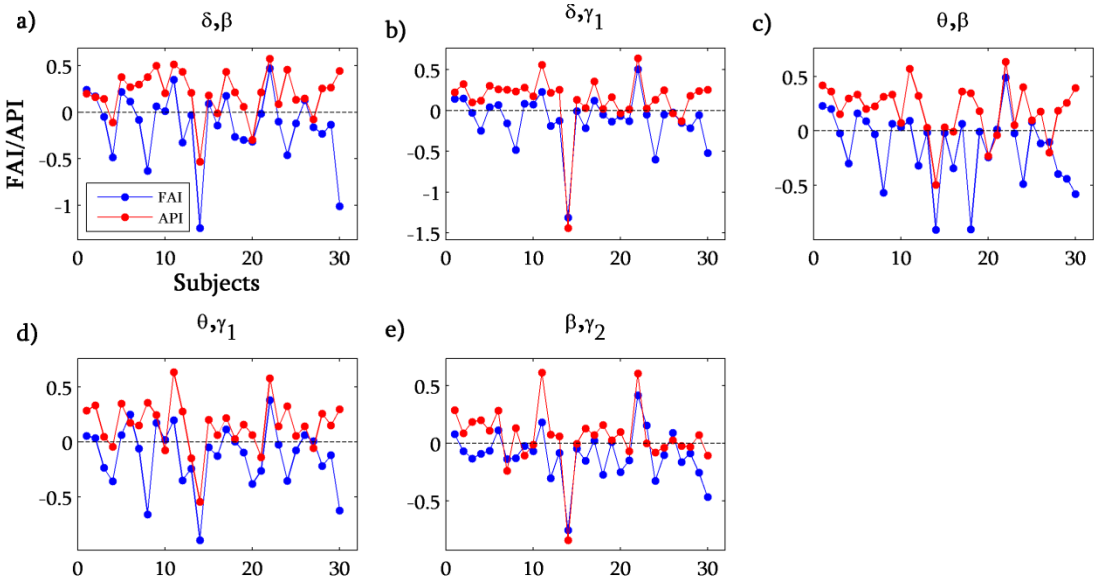

Fig. 6

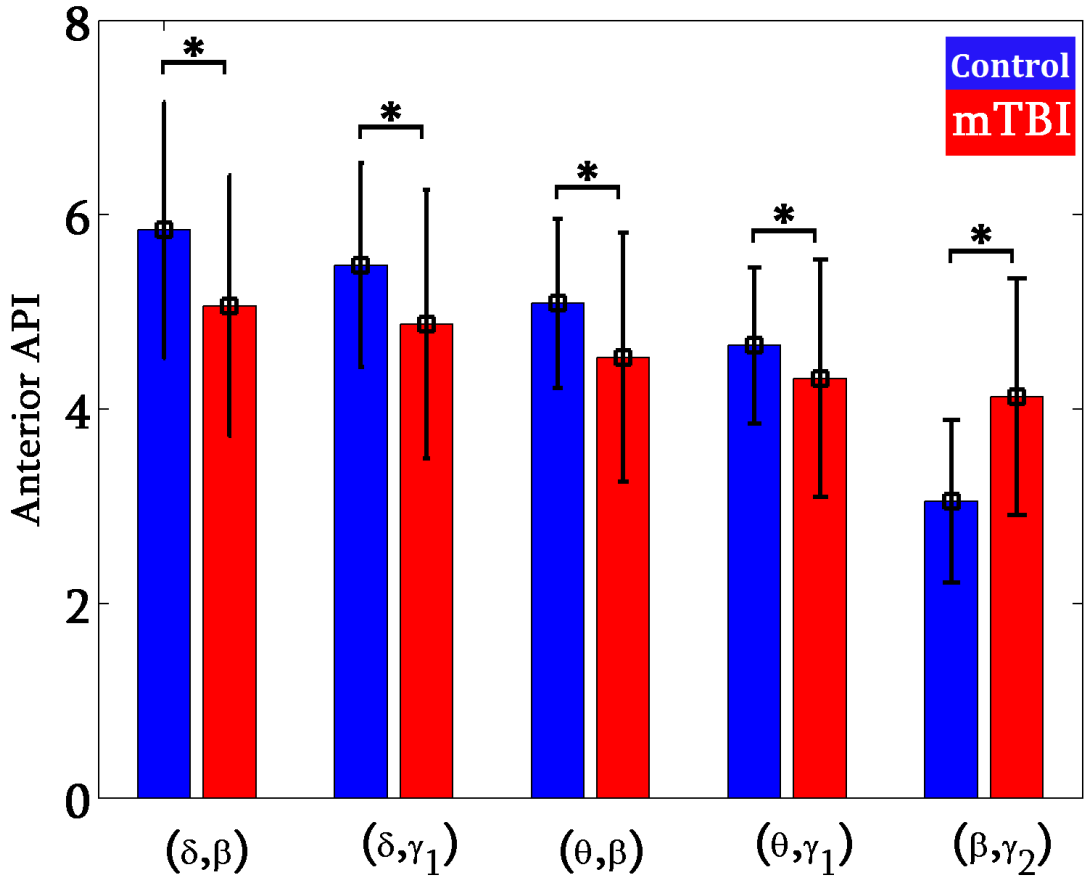

Fig. 7

Table 1. Summary of classification performance based on k-NN, ENS, and ELM classification.

	Accuracy (%)		
	k-NN	ENS	ELM
δ, β	91.25 ± 13.24	93.33 ± 11.65	90 ± 8.61
δ, γ_1	93.75 ± 6.58	96.67 ± 7.02	76.67 ± 19.56
θ, β	92.5 ± 8.74	90 ± 8.61	76.67 ± 21.08
θ, γ_1	93.75 ± 10.62	90 ± 11.65	83.33 ± 13.61
β, γ_2	93.75 ± 10.62	96.67 ± 7.03	91.67 ± 8.78
	Sensitivity (%)		
δ, β	94 ± 13.5	93.33 ± 21.08	87.5 ± 13.18
δ, γ_1	98 ± 6.32	100 ± 0	82.33 ± 20.95
θ, β	96 ± 8.43	93.33 ± 14.05	75.5 ± 23.52
θ, γ_1	96 ± 12.65	90 ± 22.5	94.17 ± 12.45
β, γ_2	94 ± 13.5	96.67 ± 10.54	95 ± 10.54
	Specificity (%)		
δ, β	86.67 ± 23.31	93.33 ± 14.05	97.5 ± 7.91
δ, γ_1	86.67 ± 17.21	93.33 ± 14.05	74.33 ± 30.7
θ, β	86.67 ± 17.21	86.67 ± 17.21	87.5 ± 22.65
θ, γ_1	90 ± 22.5	90 ± 16.1	81.17 ± 17.12
β, γ_2	93.33 ± 14.05	96.67 ± 10.54	92.5 ± 12.08

Table 2: Number of mTBI subjects showing asymmetric FAI and API values between the left and right hemisphere and between anterior and posterior brain regions.

	δ,β	δ,γ_1	θ,β	θ,γ_1	β,γ_2
FAI (left/right)	11/19	9/21	11/19	12/18	8/22
API (anterior/ posterior)	25/5	26/4	25/5	24/6	18/12

Graphical abstract